



Retrieving tropospheric NO₂ vertical column densities around the city of Beijing and estimating NO_x emissions based on car MAX-DOAS measurements

Xinghong Cheng¹, Jianzhong Ma¹, Junli Jin², Junrang Guo¹, Yuelin Liu³, Jida Peng⁴,
5 Xiaodan Ma⁵, Minglong Qian⁶, Qiang Xia⁶, Peng Yan²

¹State Key Lab of Severe Weather & Key Laboratory for Atmospheric Chemistry, Chinese Academy of Meteorological Sciences, Beijing 100081, China

²CMA Meteorological Observation Centre, Beijing 100081, China

³College of Architecture and Environment, Sichuan University, Chengdu 610065, China

10 ⁴Meteorological Institute of Fujian, Fuzhou 350001, China

⁵Nanjing University of Information Science and Technology, Nanjing 210044, China

⁶China National Huayun Technology Development Corporation, Beijing 100081, China

Correspondence to: Xinghong Cheng (cxingh@cma.gov.cn) and Jianzhong Ma (majz@cma.gov.cn)

Abstract. We carried out 19 city-circle-around car MAX-DOAS experiments on the 6th Ring Road of
15 Beijing in January, September, and October 2014. The tropospheric vertical column densities (VCDs) of
NO₂ were retrieved from measured spectra obtained by the multi-axis differential optical absorption
spectroscopy (MAX-DOAS) technique and used to estimate the emissions of NO_x (\equiv NO + NO₂) from
urban Beijing during the experimental periods. The offline LAPS-WRF-CMAQ model system was used
to simulate the wind fields by assimilation of observational data and calculate the NO₂-to-NO_x
20 concentration ratios, both of which are also needed for the estimation of NO_x emissions. The NO_x
emissions in urban Beijing for the different seasons derived from the car MAX-DOAS measurements in
this study were compared to the multi-resolution emission inventory in China for 2012 (MEIC 2012).
Our car MAX-DOAS measurement results showed higher NO₂ VCD in January than in the other two
months and typically larger NO₂ VCD at the southern parts of the 6th Ring Road than at the northern
25 parts. The wind field had obvious impacts on the spatial distribution of NO₂ VCD, with the mean NO₂
VCD along the 6th Ring Road typically being higher under the south wind than under the north wind. In
addition to the seasonal difference, the journey-to-journey variations of estimated NO_x emissions rates
(E_{NOX}) were large even within the same month, mainly due to uncertainties in the calculations of wind
speed, the ratio of NO₂ and NO_x concentration, and the decay rate of NO_x from the emission sources to
30 the measured positions under different meteorological conditions. The ranges of E_{NOX} during the heating



and non-heating periods were 28.7×10^{25} to 60.0×10^{25} molecules s^{-1} and 7.7×10^{25} to 24.8×10^{25} molecules s^{-1} , respectively. The average E_{NOx} values in the heating and non-heating periods were 43.0×10^{25} molecules s^{-1} and 13.9×10^{25} molecules s^{-1} , respectively. The uncertainty range of E_{NOx} was 16.4–33.2%. The monthly emission rates from MEIC 2012 are found to be lower than the estimated E_{NOx} , particularly in January. Our results provide important information and datasets for the validation of satellite products and also show how car MAX-DOAS measurements can be used effectively for dynamic monitoring and updating of the NO_x emissions from megacities such as Beijing.

1. Introduction

Over the past decade, serious haze weather has occurred frequently in autumn and winter in Beijing due to massive anthropogenic emissions from the consumption of fossil fuels and other sources (He et al., 2013; Zhang et al., 2013). High concentrations of aerosol particulate matter with dynamic diameter smaller than $2.5 \mu m$ ($PM_{2.5}$) threaten public health (Cao et al., 2014), disturb traffic operation by affecting visibility, and result in changes to the weather and climate because of scattering and absorption of solar radiation (Liao et al., 2015; Cheng et al., 2017). Measurements have shown that organic matter (OM), sulfate, nitrate, and ammonium made up more than 78% of the $PM_{2.5}$ in January 2013 in Beijing (Huang et al., 2014). Fractions of nitrate in $PM_{2.5}$ have obviously increased recently with the control of industry and coal in the Beijing-Tianjin-Hebei region, which has reduced SO_2 emissions and the ratio of sulfate in $PM_{2.5}$. Recent research (Tan et al., 2018) based on the aerosol observations at the campus of Peking University in 2014 revealed that aerosol pollution is nitrate-driven in spring and early fall and OM-driven in late fall and winter. The researchers suggested that nitrate formation was more significant than sulfate formation during severe pollution episodes in Beijing. Therefore, studies on the spatiotemporal variation of gaseous precursors of nitrate are very important for understanding the aerosol formation and its influencing factors. NO and NO_2 (together denoted as NO_x) form primarily in combustion processes, and the conversion between NO and NO_2 in the atmosphere is very rapid.

Emission inventories are usually developed by the so-called bottom-up approach, which is based on combinations of activity statistics (such as energy consumption and industrial production) and source- or region-specific emission factors (Hao et al., 2002; Zhang et al., 2007; Zhao et al., 2012; Streets et al., 2013). However, there are high uncertainties in bottom-up emissions inventories associated with the statistics,



emissions factors, temporal allocation profiles, and grid allocation factors (Ma and Van Aardenne, 2004; Zhao et al., 2012). Moreover, estimating “current” emissions by the bottom-up methodology is fundamentally difficult because publication of basic statistics is generally a couple of years behind. The top-down constraint is a useful supplement to bottom-up estimates, which are subject to uncertainties in
65 emissions factors and emissions activities (Streets et al., 2013). Inverse modeling, in which emissions are optimized to reduce the differences between simulated and observed data, is a powerful method that solves the problems of the bottom-up approach. Recently, its application to the estimation of NO_x emissions has been widely reported. NO_x emission rates are derived by constraining satellite observations using the relationship between model-simulated NO₂ vertical column density (VCD) and
70 primary NO_x emission estimates from the bottom-up approach (Martin, 2002; Jaegle' et al., 2005; Kononov et al., 2006; Wang et al., 2007; Lin et al., 2012; Zyrichidou et al., 2015). Nevertheless, errors and uncertainties still exist in the retrieval of satellite data, and these lead to a large decrease in precision, particularly in highly polluted regions such as Beijing and its surroundings (Ma et al., 2013a; Jin et al., 2016). Uncertainties can arise from noise, surface albedo, cloud blocks, profile shape, interference from
75 ozone absorption, correlations with other retrieved parameters, fitting wavelength window, and so forth. Air mass factor (AMF) errors can produce additional errors during the conversion process from the slant to vertical columns. Therefore, comprehensive ground-based measurements of the tropospheric columns and vertical profiles of NO₂ are quite important and necessary to evaluate and validate satellite retrieval products.

80 MAX-DOAS (Multi-Axis Differential Optical Absorption Spectroscopy) is a new ground-based remote sensing technique developed during the last decade. It makes use of the scattered sunlight measured from horizontal through zenith direction to retrieve the VCD and profiles of trace gases and aerosols with relatively high sensitivity in the lower atmosphere (Hönninger et al., 2004; Wagner et al., 2004; Platt and Stutz, 2008). MAX-DOAS has been extensively used to derive tropospheric column
85 information of NO₂ and some other pollutants in various regions (Wittrock et al., 2004; Brinkma, et al., 2008; Irie et al., 2008; Vlemmix et al., 2010; Li et al., 2013; Hendrick et al., 2014). Mobile- (or car-) MAX-DOAS measurements have been used to quantify NO_x emissions from cities and regions such as Beijing (Johansson et al., 2008), Mexico (Johansson et al., 2009), Mannheim and Ludwigshafen (Ibrahim et al., 2010), Deli (Shaiganfar et al., 2011), Shanghai (Wang et al., 2012), North China (Wu et al., 2018).
90 Compared to ground-based observations at a fixed site, car-MAX-DOAS measurements can provide



information on the spatial distribution of pollutants, which is important for explaining the urban/regional representativeness of satellite observations over megacities such as Beijing. Moreover, due to the rapid expansion of urban area and increasing energy consumption, both locations and strength of emission sources in Beijing may have changed significantly. Therefore, intensive Car-MAX-DOAS measurement campaigns are still needed to estimate the emissions of NO_x in Beijing. Mean wind speed and wind direction along the ring road during the sampling periods are usually used to estimate NO_x emissions in the previous studies. Since wind field changes rapidly due to local circulation and then results in uncertainties in quantification of NO_x emissions (Johansson et al., 2008; Shaiganfar et al., 2011, 2017; Davis, et al., 2019), refined and accurate simulations of wind fields are needed for the accurate emission estimate.

In this study, we estimated the total NO_x emissions from urban Beijing based on the VCD of NO₂ obtained from intensive car MAX-DOAS measurements on the 6th Ring Road of Beijing in January, September, and October of 2014. The offline LAPS-WRF-CMAQ model system with data assimilation method was used to derive wind speed, wind direction, and NO₂/NO_x concentration ratios, which are needed to estimate total urban NO_x emissions based on car MAX-DOAS measurements. This paper is organized as follows: Section 2 describes the intensive car MAX-DOAS experiment and the retrieval method for deriving tropospheric NO₂ VCD, the model system used to simulate wind field and the ratios of NO₂ and NO_x, and the method used to quantify total NO_x emissions. Section 3 presents the results of the NO₂ VCD and the estimated NO_x emissions as well as their uncertainties due to simulated errors in the wind field. Conclusions are provided in Section 4.

2. Theory, experimental, and method

2.1 Formula to estimate urban NO_x emissions

The complete NO₂ flux F_{NO_2} across the urban Beijing area encircled by the driving route S is estimated according to the method of Ibrahim et al. (2010).

$$F_{NO_2} = \oint_S VCD_{NO_2}(s) \cdot \bar{w} \cdot \bar{n} \cdot ds \quad (1)$$

Here $VCD_{NO_2}(s)$ is the NO₂ VCD at the sampling position within the driving route; \bar{n} indicates the normal vector parallel to the Earth's surface and orthogonal to the driving direction at the position of the driving route; \bar{w} is the average wind vector within the NO₂ layer, which is denoted by wind speed at the height of 10 m. We carried out car MAX-DOAS measurements along closed driving routes around large



emissions sources, i.e., the 6th Ring Road of Beijing (Fig. 1).

According to the calculation method of Ibrahim et al. (2010), the complete NO_x emissions from the encircled areas are determined considering the partitioning between NO and NO_2 (c_L) and the finite lifetime of NO_x (c_τ).

$$125 \quad E_{\text{NO}_x} = c_L \cdot c_\tau \cdot F_{\text{NO}_2} \quad (2)$$

$$c_L = \frac{c_{\text{NO}_x}}{c_{\text{NO}_2}} \quad (3)$$

Here c_L is simply the ratio of NO_x (C_{NO_x}) and NO_2 (C_{NO_2}) bulk concentration in the polluted layer which are simulated by the CMAQ model in this study. It is a function of the Leighton ratio ($L=[\text{NO}]/[\text{NO}_2]$), $c_L=1+L$. c_τ describes the decay of NO_x from the emission sources to measured positions. c_τ can be
130 estimated from the NO_x lifetime τ , which is the reciprocal of the product of reaction rate coefficient k ,
OH concentration (C_{OH}) and air density (M)(Ma et al., 2013), and transport time t , which is the distance
between emission source and sampling point r divided by the wind speed w .

$$c_\tau = e^{\frac{t}{\tau}} = e^{\frac{r/w}{\tau}} \quad (4)$$

$$\tau = \frac{1}{k \cdot C_{\text{OH}} \cdot M} \quad (5)$$

135 We averaged our model simulated quantities over the urban area for the NO_x lifetime τ , used the simulated wind speed at sampling position as w , and computed the distance between the sampling position and the center of the city of Beijing for r .

2.2 Car MAX-DOAS measurements

2.2.1 Instrument and experiment

140 We measured and retrieved tropospheric NO_2 VCD along the sixth ring road of Beijing (hereafter referred to as 6th Ring Rd) in January, September, and October of 2014 using a Mini MAX-DOAS instrument settled on the vehicle.

The instrument, manufactured at Hoffmann Messtechnik GmbH, Germany, is a fully automated, light-weighted spectrometer designed for the spectral analysis of scattered sunlight by the MAX-DOAS
145 technique (Hönninger et al., 2004). The same type of instrument was used in previous studies, including long-term site measurements in Beijing (Ma et al., 2013a) and a car MAX-DOAS observational journey in Europe (Wagner et al., 2010a). For this study, the instrument was mounted on the roof of a car. Inside the car, two 12V DC batteries alternatively supplied electronic power for the running of instruments and



a laptop computer, with a script run by the DOASIS software (Kraus, 2001b) to control the measurement
150 process and the recording of spectra. The temperature of the spectrograph was set to be maintained at –
5°C in January and at 0°C in September and October, well below the ambient temperatures during the
experimental days of the study. The signal spectra of dark current and electronic offset were measured
each day before and after the field experiment on the road, with 10000 msec and 1 scan for dark current
measurements and 3 msec and 1000 scans for electronic offset measurements. Measurements were made
155 alternatively at 30° and 90° elevation angles, with an integration time of about 1 min for each elevation
angle.

The instrument onboard the car was operated to measure scattered sunlight from the driving forward
direction. There were no high buildings on both sides of the 6th Ring Rd., and the measurements were
made at a wide-field view. The driving speed was typically controlled at 80–90 km h⁻¹, and it generally
160 took about 2.0–2.5 h to complete one circle (about 187 km) around the 6th Ring Rd. Figure 1 shows the
driving route of the car MAX-DOAS experiment on a map of Beijing. For this study, the field
experiments were carried out on 14 selected days, with one or two circle journeys each day. In total, there
are 19 circling journeys available. The sampling periods in this experiment and the meteorological
conditions are listed in Table 1. In most cases, the meteorological conditions changed slightly within one
165 circling journey period. The average wind speeds for experimental days in January, September, and
October were 2.5, 2.5, and 2.4 m s⁻¹, the corresponding total cloud fractions were 4.9, 7.5, and 4.2, and
the mean planetary boundary layer (PBL) heights were 192, 188, and 238 m, respectively. The dominant
wind directions in the three months were much more variable, including north, south, and other directions.

2.2.2 Spectral retrieval

170 The retrieval of NO₂ slant column densities (SCDs) is based on the DOAS method (Platt, 1994). The
WinDOAS software (Fayt and Van Roozendael, 2011) was adopted to analyze the spectra in the 400-
431 nm range on a daily basis. The Fraunhofer reference spectrum (FRS) was selected among the
measured spectra at the 90° elevation angle each day by two steps: first, a spectrum measured around
noon was chosen; second, the spectrum corresponding to the minimum NO₂ SCD derived in the
175 preliminary analysis using the FRS from the first step was finally selected. The cross sections of NO₂ at
294 K (Vandaele et al., 1998), O₃ at 221 K (Burrows et al., 1999), and the Oxygen dimmer O₄ at 298 K
(Greenblatt et al., 1990), as well as a FRS, a Ring spectrum calculated from the FRS by DOASIS (Kraus,



2001a) and a polynomial of third order were included in the spectral fitting process. Figure 2 shows an example of our spectral analysis for a measurement on 18 January 2014, 11:39:38 BJT. As shown in the figure, the atmospheric NO₂ absorption structure can be clearly extracted from the measured spectra.

2.2.3 Derivation of tropospheric NO₂ VCD

The trace gas VCD in the troposphere can be calculated using its SCD divided by the air mass factor (AMF) at an elevation angle, α :

$$\text{VCD}_{\text{trop}} = \frac{\text{SCD}_{\text{trop}}(\alpha)}{\text{AMF}_{\text{trop}}(\alpha)} \quad (6)$$

For the site MAX-DOAS measurements, a FRS from the same elevation sequence was used in most cases, and the stratospheric absorption can be assumed to be the same during one elevation sequence. Therefore, the VCD_{trop} can be calculated by extending Eq. 1 to Eq. 2 using the so-called differential tropospheric slant column density (DSCD_{trop}(α) = SCD_{trop}(α) - SCD_{trop}(90°)) divided by the differential air mass factor (DAMF_{trop}(α) = AMF_{trop}(α) - AMF_{trop}(90°)):

$$\text{VCD}_{\text{trop}} = \frac{\text{DSCD}_{\text{trop}}(\alpha)}{\text{DAMF}_{\text{trop}}(\alpha)} = \frac{\text{DSCD}_{\text{meas}}(\alpha)}{\text{DAMF}_{\text{trop}}(\alpha)} \quad (7)$$

with DSCD_{meas}(α) = SCD_{meas}(α) - SCD_{ref} (Wagner et al., 2010b; Ma et al., 2013a).

For the car MAX-DOAS measurements, the trace gas concentrations can change significantly during one measurement sequence and thus the dependence of retrieved trace gas DSCDs on the elevation angle may not be so regular as for the site measurements. Therefore, it would be a better choice to use a single FRS for the analysis of all the spectra measured along the driving route (Wagner et al., 2010b). According to Wagner et al. (2010b), Eq.1 can be further extended to

$$\text{VCD}_{\text{trop}} = \frac{\text{DSCD}_{\text{meas}}(\alpha) - \text{DSCD}_{\text{offset}}}{\text{AMF}_{\text{trop}}(\alpha)} \quad (8)$$

where DSCD_{offset} depends on the solar zenith angle (SZA) and thus local time, t_i . For each elevation sequence i during the individual measurement day, DSCD_{offset} is calculated from a single pair of measurements with

$$\text{DSCD}_{\text{offset}}(t_i) = \frac{\text{AMF}_{\text{trop}}(90^\circ) \cdot \text{DSCD}_{\text{meas}}(\alpha, t_i) - \text{AMF}_{\text{trop}}(\alpha) \cdot \text{DSCD}_{\text{meas}}(90^\circ, t_i)}{\text{AMF}_{\text{trop}}(\alpha) - \text{AMF}_{\text{trop}}(90^\circ)} \quad (9)$$

The time series of the calculated DSCD_{offset}(t_i) in this study could be fitted by a low-order polynomial, e.g., $P(x) = a_0 + a_1 \cdot x + a_2 \cdot x^2$, as a function of time. The fitted polynomial then represents the best guess for DSCD_{offset} and can be used to calculate the VCD_{trop} from Eq. 3. In this study, the AMF was calculated by the geometry approximation, that is:



$$\text{AMF}_{\text{trop}}(\alpha) \approx \frac{1}{\sin(\alpha)} \quad (10)$$

As an illustration, Figure 3 shows the changes of individual NO_2 $\text{DSCD}_{\text{meas}}$ and $\text{DSCD}_{\text{offset}}$ for 30° elevation angle of each sequence as a function of time on 18 January 2014. A second order polynomial fitted from individual $\text{DSCD}_{\text{offset}}$ data points as shown in Fig. 3 tends to converge against a much more
210 stable average $\text{DSCD}_{\text{offset}}$ value.

2.2.4 Calculation of monthly average NO_2 VCD

To investigate the differences in the spatial distribution of NO_2 VCD among the three months, we computed the monthly average NO_2 VCD for every sampling point along the 6th Ring Rd of Beijing in January, September, and October, 2014. Firstly, we used the locations of all sampling points on the
215 morning of September 23 as the reference point for the calculation of NO_2 VCD monthly average, with the most sampling sites (98 points) for all observation periods. Then, we calculated the monthly average value at each reference point using the data of the nearest sampling point. The distance from the nearest sampling point to a reference point was less than 1.5 km.

2.3 LAPS-WRF-CMAQ model simulation

2.3.1 Model setup and data 220

To quantify the NO_x emissions in Beijing more accurately, refined simulations of the wind field and NO_2 to NO_x concentration ratio were needed. In this study, we utilized the offline LAPS-WRF-CMAQ model system with high spatiotemporal resolution and data assimilation technique to obtain the refined wind speed and wind direction and an accurate ratio of NO_2 and NO_x concentration during the car MAX-
225 DOAS experiments. The aforementioned model system includes three components: the LAPS model (Albers et al., 1996), the WRF model (Michalakes et al., 2004), and the CMAQ model (Dennis et al., 1996). Simulation of wind speed and direction is improved by the LAPS-WRF model, which assimilates observed data at the surface and high layers using the one-dimensional and three-dimensional variational assimilation method (Albers et al., 1996). The CMAQ model is used to simulate temporal-spatial
230 distribution of NO_2 and NO concentration. The Local Analysis and Prediction System (LAPS), developed by the NOAA Earth System Research Laboratory, is used in many numerical weather forecast centers around the world. It is a mesoscale meteorological data assimilation tool that employs a suite of observations to generate a realistic, spatially distributed, time-evolving, threedimensional representation



of atmospheric features and processes (McGinley et al., 1991). The three-dimensional realistic
235 meteorological analyses field can be used as the initial condition of the WRF model and improve the
simulation of wind field. WRF is a mesoscale numerical weather prediction system designed for both
atmospheric research and operational forecasting needs. CMAQ is an air-quality model developed by the
U.S. Environmental Protection Agency's Atmospheric Science Modeling Division. It consists of a suite
of computer programs for modeling air quality issues, including reactive gases such as NO₂, NO, SO₂,
240 O₃, and others, particulate matter (PM), air toxics, acid deposition, and visibility degradation.

This study focused on Beijing at a horizontal resolution of 4 km × 4 km with 31 vertical layers of
varying thickness (between the surface and 50 hPa) using a triple-nested simulation technique. The
horizontal resolutions of the three sets of grids were 36 km, 12 km, and 4 km, respectively (Fig. S1a),
and the output temporal interval was 1 h. The LAPS-WRF simulations were driven by FNL/NCEP
245 analysis data every 6 h during the car MAX-DOAS experiments, with a spatial resolution of 1° × 1°. In
addition, to improve the simulation of wind field and NO₂ and NO concentrations, many meteorological
data of the same periods, such as wind speed, wind direction, air temperature, and relative humidity,
observed at 2400 surface weather stations and by 120 radiosonde stations were assimilated into the initial
field of the WRF model using the one-dimensional and three-dimensional variational assimilation
250 method in the LAPS model. The CMAQ model uses the MEIC 2012 with 0.25° × 0.25° resolution (Zhang
et al., 2009; Li et al., 2017). Hourly gridded MEIC emission datasets at a horizontal resolution of 4 km
× 4 km for the CMAQ model were generated by the Sparse Matrix Operator Kernel Emissions (SMOKE)
modeling system (UNC, 2014) using reasonable temporal and spatial allocation coefficients (Cheng et
al., 2017). Meteorological outputs from the WRF simulations were processed to create model-ready
255 inputs for CMAQ using the Meteorology–Chemistry Interface Processor (MCIP) (Otte and Pleim, 2010).
The chemical mechanism is CB05, and the boundary conditions of trace gases consist of idealized,
Northern Hemispheric, mid-latitude profiles based on results from the NOAA Agronomy Lab Regional
Oxidant Model. The model simulation was started one day before the first day of the experiment to avoid
the spin-up problem and improve the simulation accuracy.

260 2.3.2 Validation of simulated surface wind and NO₂

Modeled wind speeds and directions were validated by observation data from four weather stations in
Beijing. The observed hourly wind speed and direction data at the meteorological stations, shown in



Figures S2 and S3, were obtained from the China Meteorological Administration. The four stations are the Nanjiao (NJ), Tongzhou (TZ), Mentougou (MTG), and Shunyi (SY) meteorological stations, which
265 represent the south, east, west, and north area of Beijing, respectively. It was shown that the temporal variation in simulated wind speed at the four stations were consistent with the observations, but the simulations were higher than the observations (Fig. S2). To calculate the E_{NO_x} accurately, we corrected the simulated wind speed using the observation data from the four weather stations. Specifically, we computed the relative error of the modeled wind speed during every journey and then used it to correct
270 the simulated wind speed at all sampling points for every journey. The correlation coefficient between simulated and observed wind speeds at the four stations was 0.47, and the result passed the 99.9% significance test. The root mean square error (RMSE) was small, with a value of 1.18 m s^{-1} . Except for the MTG station, simulated wind directions at the other three stations were in accordance with the observations, particularly for the primary wind direction (Fig. S3). The primary wind direction and its
275 frequency at the MTG station were not consistent with the observations because these are affected by the complex topography near the Taihang and Yanshan mountains. Hence, the simulations of wind speed and wind direction were reliable for estimation of the NO_x emissions.

Figure S4 presents the temporal variation in simulated and observed NO_2 concentration from January 18 to October 13, 2014. The hourly measurements of NO_2 concentrations (shown in Fig. S1b) were
280 obtained from the National Environment Monitoring Station in China. In general, the temporal variation in the NO_2 simulation was consistent with the observation. The simulated values were close to the observations, except for January 21–24, September 19, and October 9–10, when NO_2 simulations were higher than the observations. The correlation coefficient between simulated and observed NO_2 concentrations was 0.73, and the result passed the 99.9% significance test (Fig. S5). The RMSE and mean
285 absolute error (MAE) were 16.14 and $19.21 \mu\text{g m}^{-3}$, respectively. Because observed NO_2 might include the NO_z component, it can lead to a systematical biases (underestimation) of NO_2 by model compared to observation (Ma et al., 2012). Thus, the simulated NO_2 concentrations and hence the ratio of NO_2 and NO_x were reliable for estimating NO_x emissions.

290 3. Results and Discussion

3.1 Tropospheric NO_2 VCD

Figure 4 presents the temporal variation in the tropospheric NO_2 VCD on the 6th Ring Rd of Beijing in



January, September, and October, 2014. In general, the NO₂ VCD in January was higher than that in other months. The highest values falling between 8×10^{16} and 13×10^{16} molecules cm⁻² occurred on January 19, 23, and 24. The mean, maximum, and minimum NO₂ VCD during the sampling periods were all larger in January than in the other two months. The mean NO₂ VCD ranged mostly from 4.5×10^{16} to 9×10^{16} molecules cm⁻² in January, but values were all lower than 4.5×10^{16} molecules cm⁻² in September and October. The NO₂ VCD values during the mornings of January 23 and October 13 were 9.05×10^{16} and 1.23×10^{16} molecules cm⁻², corresponding to the maximum and minimum values, respectively, during the 19 circling journeys. This result may be caused by higher emissions and some meteorological conditions that were unfavorable for dispersion and transport of pollutants in winter. Lower PBL height and lower wind speed suppress horizontal and vertical diffusion and transport of NO_x. Southwest and east winds are favorable for the transport of air pollutants from the south and east areas to the city of Beijing. Higher cloud cover is unfavorable for photolysis of NO₂. A similar pattern of seasonal variation in tropospheric NO₂ VCD was found previously by site MAX-DOAS measurements in Beijing (Ma et al., 2013a; Hendrick et al., 2014).

Figure 5 shows that the monthly average NO₂ VCD at most sampling points on the 6th Ring Rd were obviously higher in January than in the other two months (by a factor of two in most cases). The spatial distribution characteristics of NO₂ VCD in September were similar to those in October. In addition, the NO₂ VCD values at the northern and southern parts of the 6th Ring Rd were all larger than those in other areas for all three months. The high NO₂ VCD in the southern region was related to strong local emissions to the south of Beijing and transport from central and southern Hebei and the city of Tianjin (Meng et al., 2018). As shown in Fig. 4, the maximum journey-averaged NO₂ VCD occurred on the morning of January 23, and the minimum occurred on the morning of October 13.

We investigated the spatial distribution differences in NO₂ VCD between these two circling journeys, as shown in Fig. 6. The NO₂ VCD values on the 6th Ring Rd in the morning of January 23 were all large, particularly in the north and southwest areas, with magnitudes of 10×10^{16} to 12×10^{16} molecules cm⁻². On October 13, high NO₂ VCD was located in the southern areas, but values were lower in the northern areas. The spatial distribution differences between these two journeys were related to the high emission during the heating season in January (see section 3.2) and the impacts of the wind field. To investigate the impact of the wind field on the spatial distribution of NO₂ VCD, we used thin-grid ECWMF reanalysis data for January 23 and October 13 with a spatial resolution of $0.125^\circ \times 0.125^\circ$. Figure 7 shows



the distribution difference of wind field at 8:00 and 14:00 BJT on these two days, respectively. The NO₂ VCD was large with weak south wind and with convergence of southeast and northwest wind in Beijing and its surrounding area, but values were far smaller with strong north wind. Weak south wind and a breeze or calm wind resulted in the transport of NO₂ from the south area in Hebei Province and its accumulation on January 23. Strong north wind suppressed the transport of NO₂ from the south area on October 13. These results indicate that the wind field has large impacts on the spatial distribution of NO₂ VCD in Beijing.

Figure 8 presents the spatial distributions of wind and NO₂ VCD averaged for the three different wind fields. The mean NO₂ VCD at most sampling points along the 6th Ring Rd was obviously higher under the south wind field than under the north wind. High NO₂ emission in the three months was located within the 5th Ring Rd of Beijing (Fig. 10), and the background concentrations of NO₂ VCD in the north and south areas were remarkably different due to the impacts of emission sources from south areas of Beijing, such as Hebei Province. Hence, southerly wind can transfer air pollutants from the southern area to Beijing and lead to high NO₂ flux and NO_x emission, whereas impacts of north wind on NO₂ flux and NO_x emission are smaller because the background concentration of NO₂ VCD in north of Beijing is lower. Convergence of the wind field in the south parts of the 6th Ring Rd is favorable to accumulation of NO₂ from the surrounding area to the southern parts of the ring road.

3.2 Quantification of NO_x emissions

To estimate the NO₂ fluxes (F_{NO_2}) and E_{NO_x} accurately, we used the data from 10 circling journeys (Table 1), for which the RMSEs of simulated wind speeds at the four weather stations were all less than 1.5 m s⁻¹. In addition, NO₂ VCD measurements at the sampling points outside of the 6th Ring Rd during 11 circling journeys were not used to quantify F_{NO_2} and E_{NO_x} . Figure 9 shows the journey-to-journey variation in estimated F_{NO_2} and E_{NO_x} over Beijing for the 10 circling journeys in January, September, and October, 2014. The F_{NO_2} fell in between 1.13×10^{25} and 11.35×10^{25} molecules s⁻¹. The ranges of E_{NO_x} during the heating (January) and non-heating (September and October) periods were 28.7×10^{25} to 60.0×10^{25} molecules s⁻¹ and 7.7×10^{25} to 24.8×10^{25} molecules s⁻¹, respectively. The average E_{NO_x} values in the heating and non-heating periods were 43.0×10^{25} molecules s⁻¹ and 13.9×10^{25} molecules s⁻¹, respectively. In general, the journey-to-journey variation patterns of F_{NO_2} and E_{NO_x} were consistent with that of the mean NO₂ VCD. In other words, the estimate of E_{NO_x} was determined mainly by the NO₂



VCD. Seasonal variation characteristics of the estimated E_{NO_x} were obvious. Specifically, the total E_{NO_x} was higher in January than in the other two months. The average E_{NO_x} in the heating period was about 3.1 times those in the non-heating period.

355 In addition to the seasonal differences, the journey-to-journey variation in estimated E_{NO_x} were large even within the same month, mainly due to uncertainties in the calculations of wind speed, ratio of NO_2 and NO_x concentration, and decay rate of NO_x from the emission sources to the measured positions under different meteorological conditions. In addition to the NO_2 VCD, wind speed, and wind direction at the sampling points, the estimated NO_x emission rate is obviously affected by the Leighton ratio of
360 NO and NO_2 concentration and the lifetime of NO_x (Valin, et al., 2013). Thus, the estimated NO_x emission rate could be very large even if the NO_2 VCD was small, such as in the case of January 27. It should be noted that the mean wind speed on January 27 was relatively small and led to higher c_τ , meanwhile, the ratios of NO_x and NO_2 were relatively large, so E_{NO_x} on January 27 was large although F_{NO_2} was relatively small. Thus, if c_τ and c_L are simultaneously larger, higher E_{NO_x} occurs. However, if
365 only one factor is larger and the other is smaller, such as higher c_τ and lower c_L as on January 18, the morning and afternoon of September 14, and the morning of October 13, E_{NO_x} is lower.

3.3 Comparisons with MEIC inventory and other estimates

We compared the estimated NO_x emission with the multi-resolution emission inventory in China (MEIC) released by Tsinghua University for 2012 (MEIC 2012) (Zhang et al., 2009; Zhang et al., 2012). The
370 horizontal resolution of MEIC 2012 is $0.25^\circ \times 0.25^\circ$, and five sectors, agriculture, industry, power, residents, and transportation, are included.

Figure 10 presents the spatial distributions of NO_x emission rates over Beijing in January, September, and October, 2012, from MEIC. A high NO_x emission zone was located within the 5th Ring Rd of Beijing, and a low emission zone occurred in other areas. The NO_x emissions in January were obviously larger
375 than those in the other two months. The concentrated distribution of NO_x emission sources within the 5th Ring Rd of Beijing indirectly indicates the applicability of Eq. (1) to estimate the NO_x emission rates from the car MAX-DOAS measurements on the 6th Ring Rd in this study.

Figure 11 shows the journey-to-journey estimated NO_x emission rates from car MAX-DOAS measurements in January, September, and October, 2014 (denoted as E_{NO_x}), and the corresponding
380 monthly averaged NO_x emission rates from the MEIC 2012 for the same region within the 6th Ring Rd



of Beijing (hereafter expressed as MEIC_Month). In most cases, the MEIC_Month was lower than the estimated E_{NOX} , particularly in January. The differences between the estimated E_{NOX} and the MEIC_Month during some journeys were remarkably large. The differences between the E_{NOX} and MEIC 2012 during the 10 journeys may be caused by (1) the interannual differences in emission inventory, (2) 385 the different timescales of the two emission estimates, (3) the uncertainty of the estimated E_{NOX} and MEIC 2012, (4) inconsistency of wind field during the period of measurements, (5) extra transfers from source areas other than urban Beijing, and so on. Firstly, the E_{NOX} in this study was estimated for the year 2014, whereas the MEIC 2012 was established for the year 2012. Secondly, our results represented only the conditions during a few measurements during daytime, whereas the MIEC 2012 denoted monthly 390 average conditions. Thirdly, the uncertainty of MEIC 2012 is large, particularly in autumn and winter (Li *et al.*, 2017; Meng *et al.*, 2018). Fourthly, the emission estimation method used in this study assumes that the wind field is constant during the period of measurements and that the wind speed is also sufficiently high that the transport across the encircled area is fast compared to the atmospheric lifetime of the trace gas (Ibrahim *et al.*, 2010). However, the wind field during some journeys could have changed 395 systematically and been convergent or divergent in some areas of Beijing, as marked as other type of wind field in Table 1. Ibrahim *et al.* (2010) also pointed out that systematic changes during the period of measurements can become important to the emission estimate, particularly if measurements with high trace gas VCD are accompanied by strong deviations of the actual wind speed (or direction) from the assumed average values. For example, on the morning of January 27, the highest NO_2 VCD was measured, 400 and the wind field changed during the measurement journey. In such cases, the systematic changes in wind speed and direction can lead to additional uncertainties in E_{NOX} . Finally, because southerly wind can bring NO_x emitted in the south-central regions of Hebei Province to Beijing, the E_{NOX} from car MAX-DOAS measurements will be overestimated under south wind conditions.

Figure 11 also shows the uncertainty of E_{NOX} , calculated from the errors of measured NO_2 VCD, 405 simulated wind speed, c_L and c_τ according to the error transfer formula of relative deviation. The standard deviation (STD) of wind speed over a period of time can provide a bound for the related uncertainties of the emission estimate (Ibrahim *et al.*, 2010). Therefore, we first computed the uncertainty of F_{NO_2} based on the STD of the corrected wind speed and the measurement error of NO_2 VCD (about $\pm 10\%$, Ma *et al.*, 2013a) for each journey. Then, we calculated STD of c_τ according to the first derivative 410 of equation (4) and the monthly STD of c_L using its regional average data within the 6th Ring Rd of



Beijing during all journeys in each month. We used the identical STD of c_L for each journey in the same month to calculate of the uncertainty of E_{NOX} . The results showed that the STD ranges of wind speed, c_L and c_t were 0.13–1.30 $m s^{-1}$, 0.11–0.37, and 0.17–1.97, respectively. The uncertainty range of E_{NOX} was 16.4–33.2%.

415

4. Conclusion and Discussion

We carried out 19 city-circle-around car MAX-DOAS experiments on the 6th Ring Rd of Beijing in January, September, and October, 2014. The VCD of NO_2 was retrieved and the temporal and spatial distributions were investigated. Then the NO_X emission rates in urban Beijing were estimated using the measured NO_2 VCD together with the refined wind fields, NO_2 to NO_X ratios, and NO_2 lifetimes simulated by the LAPS-WRF-CMAQ model system, and the results were compared to the emission rates from the MEIC inventory 2012.

The mean, maximum, and minimum NO_2 VCD values during the sampling periods in January were all larger than those in the other two months, mainly due to higher emissions in winter. The mean NO_2 VCD was typically larger at the southern parts of the 6th Ring Road than northern parts because weak south wind resulted in the transport and accumulation of NO_2 from southern areas in Hebei Province and strong north wind suppressed the transport of NO_2 from the southern area. Such inhomogeneous distributions of tropospheric NO_2 VCD bring a challenge for validation of satellite products for Beijing as well as other megacities.

The journey-to-journey variation in estimated E_{NOX} were large, even within the same month, mainly due to uncertainties in the calculation of wind speed, the ratio of NO_2 and NO_X concentration, and the decay rate of NO_X from the emission sources to the measured positions under different meteorological conditions. The ranges of E_{NOX} during the heating and non-heating periods were 28.7×10^{25} to 60.0×10^{25} molecules s^{-1} and 7.7×10^{25} to 24.8×10^{25} molecules s^{-1} , respectively. The average E_{NOX} values in the heating and non-heating periods were 43.0×10^{25} molecules s^{-1} and 13.9×10^{25} molecules s^{-1} , respectively. The uncertainty range of E_{NOX} was 16.4–33.2%. The monthly emission rates in the area within the 6th Ring Rd of Beijing from MEIC 2012 were lower than the estimated E_{NOX} , particularly in January. The differences between the E_{NOX} and the monthly emission rates from MEIC 2012 may be attributable to the interannual differences in the emissions inventory, the different timescales and uncertainties of two kinds of inventory, inconsistencies of wind field during the period of measurements,



and extra transfers from source areas other than urban Beijing.

Our results showed that car MAX-DOAS measurements can be used effectively for dynamic monitoring and updating of the NO_x emissions from megacities such as Beijing. To estimate E_{NO_x} by car MAX-DOAS accurately in Beijing and other similar megacities, appropriate meteorological conditions, such as smaller fluctuations of the wind field, relatively larger wind speed, and suitable wind direction, need
445 as smaller fluctuations of the wind field, relatively larger wind speed, and suitable wind direction, need to be selected to avoid the impact of extra transfers of large emission sources from surrounding areas. In addition to the NO₂ VCD, simultaneous observations of wind speed, wind direction, and surface NO and NO₂ concentrations are recommended to reduce the uncertainties of c_T and c_L.

450 *Data availability.* The NCEP-FNL reanalysis and ECMWF are publicly available at <http://rda.ucar.edu/datasets/ds083.2/> and <https://www.ecmwf.int/en/forecasts/datasets>, respectively. The NO₂ - measurements and meteorological observations including wind speed and wind direction data are available at <http://113.108.142.147:20035/emcpublish> and <http://data.cma.cn/>, respectively. The tropospheric NO₂ VCD data derived from this study are available on the request.

455 *Author contributions.* JM and XC designed the research. JM, JJ, JG, MQ, QX, and PY contributed to the measurements, and JM performed the spectral analysis and retrieval. XC and JP designed the model experiment and performed the model simulations. XC, YL, JP, and XM contributed to the data processing and analyses. XC and JM analyzed the results and wrote the paper with inputs from all authors.

460 *Competing interests.* The authors declare that they have no conflicts of interest.

Acknowledgments. This work was supported jointly by the National Natural Science Foundation of China (91644223), the National Research Program for Key Issues in Air Pollution Control (DQGG0104), and
465 the Scientific and Technological Development Funds from the Chinese Academy of Meteorological Sciences (2018KJ042). The authors acknowledge Tsinghua University for providing the emissions inventory and the China National Environmental Monitoring Centre for providing surface PM_{2.5} observation data.



470 References

- Albers, S. C., McGinley, J. A., Birkenheuer, D., and Smart, J. R.: The local analysis and prediction system (LAPS): Analyses of clouds, precipitation, and temperature, *Wea. Forecasting*, 11, 273-287, 1996.
- Brinksmma, E. J., Pinardi, G., Volten, H., Braak, R., Richter, A., Schoenhardt, A., van Roozendael, M., Fayt, C., Hermans, C., Dirksen, R. J., Vlemmix, T., Berkhout, A. J. C., Swart, D. P. J., Oetjen, H.,
475 Wittrock, F., Wagner, T., Ibrahim, O. W., de Leeuw, G., Moerman, M., Curier, R. L., Celarier, E. A., Cede, A., Knap, W. H., Veefkind, J. P., Eskes, H. J., Allaart, M., Rothe, R., Piters, A. J. M. and Levelt, P. F.: The 2005 and 2006 DANDELIONS NO₂ and aerosol intercomparison campaigns, *J. Geophys. Res.-Atmospheres*, 113(D16), D16S46, doi:10.1029/2007JD008808, 2008.
- Burrows, J. P., Richter, A., Dehn, A., Deters, B., Himmelmann, S., Voigt, S., and Orphal, J.: Atmospheric
480 remote sensing reference data from GOME-2. temperature-dependent absorption cross-sections of O₃ in the 231-794 nm range, *J. Quant. Spectrosc. Ra.*, 61, 509-517, 1999.
- Cao, C., Jiang, W., Wang, B., Fang, J., Lang, J., Tian, G., Jiang, J., and Zhu, T. F.: Inhalable microorganisms in Beijing's PM_{2.5} and PM₁₀ pollutants during a severe smog event, *Environ Sci Technol*, 48, 1499-1507, 10.1021/es4048472, 2014.
- 485 Cheng, X., Sun, Z., Li, D., Xu, X., Jia, M., and Cheng, S.: Short-term aerosol radiative effects and their regional difference during heavy haze episodes in January 2013 in China, *Atmospheric Environment*, 165, 248-263, 10.1016/j.atmosenv.2017.06.040, 2017.
- Davis, Z. Y. W., Baray, S., McLinden, C. A., Khanbabakhani, A., Fujs, W., Csukat, C., Debosz, J. and McLaren, R.: Estimation of NO_x and SO₂ emissions from Sarnia, Ontario, using a mobile MAX-
490 DOAS (Multi-AXis Differential Optical Absorption Spectroscopy) and a NO_x analyzer, *Atmospheric Chem. Phys.*, 19(22), 13871–13889, doi:https://doi.org/10.5194/acp-19-13871-2019, 2019.
- Dennis, R., Byun, D., and Novak, J.: The next generation of integrated air quality modeling: EPA's Models-3, *Atmos. Environ.*, 30, 1925-1938, 1996.
- Fayt, C., and Van Roozendael, M.: WinDOAS 2.1 software user manual, IASB/BIRA Uccle, Belgium,
495 2011.
- Greenblatt, G. D., Orlando, J. J., Burkholder, J. B., and Ravishankara, A. R.: Absorption measurements of oxygen between 330 and 1140 nm, *J. Geophys. Res.*, 95, 18577-18582, 10.1029/JD095iD11p18577, 1990.



- Hönninger, G., von Friedeburg, C., and Platt, U.: Multi axis differential optical absorption spectroscopy (MAX-DOAS), *Atmos. Chem. Phys.*, 4, 231-254, 10.5194/acp-4-231-2004, 2004.
- Hao, J., Tian, H., and Lu, Y.: Emission inventories of NO_x from commercial energy consumption in China, 1995-1998, *Environmental Science and Technology*, 36, 552–560, 2002.
- He, H., Wang, X. M., Wang, Y. S., Wang, Z. F., Liu, J. G., and Chen, Y. F.: Formation Mechanism and Control Strategies of Haze in China, *Bull. Chin. Acad. Sci.*, 28, 344-352, 2013.
- 505 Hendrick, F., Müller, J. F., Clémer, K., Wang, P., De Mazière, M., Fayt, C., Gielen, C., Hermans, C., Ma, J. Z., Pinardi, G., Stavrou, T., Vlemmix, T., and Van Roozendaal, M.: Four years of ground-based MAX-DOAS observations of HONO and NO₂ in the Beijing area, *Atmospheric Chemistry and Physics*, 14, 765-781, 10.5194/acp-14-765-2014, 2014.
- Huang, R. J., Zhang, Y., Bozzetti, C., Ho, K. F., Cao, J. J., Han, Y., Daellenbach, K. R., Slowik, J. G., 510 Platt, S. M., Canonaco, F., Zotter, P., Wolf, R., Pieber, S. M., Bruns, E. A., Crippa, M., Ciarelli, G., Piazzalunga, A., Schwikowski, M., Abbaszade, G., Schnelle-Kreis, J., Zimmermann, R., An, Z., Szidat, S., Baltensperger, U., El Haddad, I., and Prevot, A. S.: High secondary aerosol contribution to particulate pollution during haze events in China, *Nature*, 514, 218-222, 10.1038/nature13774, 2014.
- Ibrahim, O., Shaiganfar, R., Sinreich, R., Stein, T., Platt, U., and Wagner, T.: Car MAX-DOAS 515 measurements around entire cities: quantification of NO_x emissions from the cities of Mannheim and Ludwigshafen (Germany), *Atmos. Meas. Tech.*, 3, 709-721, 10.5194/amt-3-709-2010, 2010.
- Irie, H., Kanaya, Y., Akimoto, H., Z., W., Gleason, J. F., and Bucsele, E. J.: Validation of OMI tropospheric NO₂ column data using MAX-DOAS measurements deep inside the North China Plain in June 2006 Mount Tai Experiment 2006, *Atmos. Chem. Phys.*, 8, 6577-6586, 2008.
- 520 Jaegle', L., Steinberger, L., Martin, R. V., and Chance, K.: Global partitioning of NO_x sources using satellite observations: relative roles of fossil fuel combustion, biomass burning and soil emissions, *The Royal Society of Chemistry*, 130, 407–423, 2005.
- Jin, J., Ma, J., Lin, W., Zhao, H., Shaiganfar, R., Beirle, S., and Wagner, T.: MAX-DOAS measurements and satellite validation of tropospheric NO₂ and SO₂ vertical column densities at a rural site of North 525 China, *Atmospheric Environment*, 133, 12-25, <http://dx.doi.org/10.1016/j.atmosenv.2016.03.031>, 2016.
- Johansson, M., Galle, B., Yu, T., Tang, L., Chen, D., Li, H., Li, J. X., and Zhang, Y.: Quantification of total emission of air pollutants from Beijing using mobile mini-DOAS, *Atmospheric Environment*, 42,



- 6926-6933, <http://dx.doi.org/10.1016/j.atmosenv.2008.05.025>, 2008.
- 530 Johansson, M., Rivera, C., de Foy, B., Lei, W., Song, J., Zhang, Y., Galle, B., and Molina, L.: Mobile mini-DOAS measurement of the outflow of NO₂ and HCHO from Mexico City, *Atmos. Chem. Phys.*, 9, 5647-5653, 10.5194/acp-9-5647-2009, 2009.
- Konovalov, I. B., Beekmann, M., Richter, A., and Burrows, J. P.: Inverse modeling of the spatial distribution of NO_x emissions on a continental scale using satellite data, *Atmospheric Chemistry and Physics*, 6, 1747-1770, 2006.
- 535 Kraus, S.: DOASIS, DOAS for Windows software [CD-ROM], in: Proceedings of the 1st International DOAS-Workshop, Heidelberg, Germany, 13-14 September 2001, 2001a.
- Kraus, S.: DOASIS, DOAS for Windows software [CD-ROM], in: Proceedings of the 1st International DOAS-Workshop, Heidelberg, Germany, 13-14 September 2001, 2001b.
- 540 Li, M., Liu, H., Geng, G., Hong, C., Liu, F., Song, Y., Tong, D., Zheng, B., Cui, H., Man, H., Zhang, Q., and He, K.: Anthropogenic emission inventories in China: a review, *National Science Review*, 4, 834-866, 10.1093/nsr/nwx150, 2017.
- Li, X., Brauers, T., Hofzumahaus, A., Lu, K., Li, Y., Shao, M., Wagner, T., and Wahner, A.: MAX-DOAS measurements of NO₂, HCHO and CHOCHO at a rural site in Southern China, *Atmospheric Chemistry and Physics*, 13, 2133-2151, 2013.
- 545 Liao, L., Lou, S. J., Fu, Y., Chang, W. J., and Liao, H.: Radiative forcing of aerosols and its impact on surface air temperature on the synoptic scale in eastern China, *Chin. J. Atmos. Sci. (Chin. Ver.)*, 39, 68-82, 2015.
- Lin, J. T., Liu, Z., Zhang, Q., Liu, H., Mao, J., and Zhuang, G.: Modeling uncertainties for tropospheric nitrogen dioxide columns affecting satellite-based inverse modeling of nitrogen oxides emissions, *Atmospheric Chemistry and Physics*, 12, 12255-12275, 10.5194/acp-12-12255-2012, 2012.
- 550 Ma, J., and Van Aardenne, J. A.: Impact of different emission inventories on simulated tropospheric ozone over China: a regional chemical transport model evaluation, *Atmos. Chem. Phys.*, 4, 877-887, 2004.
- Ma, J. Z., Wang, W., Chen, Y., Liu, H. J., Yan, P., Ding, G. A., Wang, M. L., Sun, J., and Lelieveld, J.: 555 The IPAC-NC field campaign: a pollution and oxidization pool in the lower atmosphere over Huabei, China, *Atmos. Chem. Phys.*, 12, 3883-3908, 10.5194/acp-12-3883-2012, 2012.
- Ma, J., Wang, W., Liu, H., Chen, Y., Xu, X., and Lelieveld, J.: Pollution plumes observed by aircraft over North China during the IPAC-NC field campaign, *Chinese Science Bulletin*, 58, 4329-4336,



- 10.1007/s11434-013-5978-9, 2013.
- 560 Ma, J. Z., Beirle, S., Jin, J. L., Shaiganfar, R., Yan, P., and Wagner, T.: Tropospheric NO₂ vertical column densities over Beijing: results of the first three years of ground-based MAX-DOAS measurements (2008–2011) and satellite validation, *Atmospheric Chemistry and Physics*, 13, 1547-1567, 10.5194/acp-13-1547-2013, 2013a.
- Martin, R. V.: An improved retrieval of tropospheric nitrogen dioxide from GOME, *Journal of Geophysical Research*, 107, 10.1029/2001jd001027, 2002.
- 565 McGinley, J. A., Albers, S., and Stamus, P.: Validation of a composite convective index as defined by a real-time local analysis system, *Wea.Forecasting*, 6, 337-356, 1991.
- Meng, K., Xu, X., Cheng, X., Xu, X., Qu, X., Zhu, W., Ma, C., Yang, Y., and Zhao, Y.: Spatio-temporal variations in SO₂ and NO₂ emissions caused by heating over the Beijing-Tianjin-Hebei Region constrained by an adaptive nudging method with OMI data, *The Science of the total environment*, 642, 543-552, 10.1016/j.scitotenv.2018.06.021, 2018.
- 570 Michalakes, J., Dudhia, J., Gill, D., Henderson, T., Klemp, J., Skamarock, W., and Wang, W.: The weather research and forecast model: software architecture and performance, the 11th ECMWF Workshop on the Use of High Performance Computing In Meteorology, George Mozdzyński, 2004.
- 575 Otte, T. L., and Pleim, J. E.: The Meteorology-Chemistry Interface Processor (MCIP) for the CMAQ modeling system: updates through MCIPv3.4.1, *Geosci. Model Dev.*, 3, 243-256, 2010.
- Platt, U.: Differential optical absorption spectroscopy (DOAS), in: *Air Monitoring by Spectroscopic Techniques*, edited by: Sigrist, M. W., Chemical Analysis Series, 127, John Wiley, New York, 27–84, 1994.
- 580 Platt, U., and Stutz, J.: *Differential Optical Absorption Spectroscopy Principles and Applications*, Physics of Earth and Space Environments, Springer, Heidelberg, 2008.
- Shaiganfar, R., Beirle, S., Sharma, M., Chauhan, A., Singh, R. P., and Wagner, T.: Estimation of NO_x emissions from Delhi using Car MAX-DOAS observations and comparison with OMI satellite data, *Atmos. Chem. Phys.*, 11, 10871-10887, 10.5194/acp-11-10871-2011, 2011.
- 585 Shaiganfar, R., Beirle, S., van der Gon, H. D., Jonkers, S., Kuenen, J., Petetin, H., Zhang, Q., Beekmann, M. and Wagner, T.: Estimation of the Paris NO_x emissions from mobile MAX-DOAS observations and CHIMERE model simulations during the MEGAPOLI campaign using the closed integral method, *Atmospheric Chem. Phys.*, 17(12), 7853–7890, doi:10.5194/acp-17-7853-2017, 2017.



- Streets, D. G., Canty, T., Carmichael, G. R., de Foy, B., Dickerson, R. R., Duncan, B. N., Edwards, D. P.,
590 Haynes, J. A., Henze, D. K., Houyoux, M. R., Jacob, D. J., Krotkov, N. A., Lamsal, L. N., Liu, Y., Lu,
Z., Martin, R. V., Pfister, G. G., Pinder, R. W., Salawitch, R. J., and Wecht, K. J.: Emissions estimation
from satellite retrievals: A review of current capability, *Atmospheric Environment*, 77, 1011-1042,
10.1016/j.atmosenv.2013.05.051, 2013.
- Tan, T., Hu, M., Li, M., Guo, Q., Wu, Y., Fang, X., Gu, F., Wang, Y., and Wu, Z.: New insight into PM_{2.5}
595 pollution patterns in Beijing based on one-year measurement of chemical compositions, *The Science
of the total environment*, 621, 734-743, 10.1016/j.scitotenv.2017.11.208, 2018.
- UNC: SMOKE v3.6 user's manual, Chapel Hill: The institute for the Environmen, 2014.
- Vandaele, A. C., Hermans, C., Simon, P. C., Carleer, M., Colin, R., Fally, S., Mérienne, M. F.,
Jenouvrier, A., and Coquart, B.: Measurements of the NO₂ absorption cross-section from 42 000 cm⁻¹
600 to 10 000 cm⁻¹ (238–1000 nm) at 220 K and 294 K, *J. Quant. Spectrosc. Ra.*, 59, 171-184, 1998.
- Valin, L. C., Russell, A. R. and Cohen, R. C.: Variations of OH radical in an urban plume inferred from
NO₂ column measurements, *Geophys. Res. Lett.*, 40(9), 1856–1860, doi:10.1002/grl.50267, 2013.
- Vlemmix, T., Piters, A., Stammes, P., Wang, P., and Levelt, P.: Retrieval of tropospheric NO₂ using the
MAX-DOAS method combined with relative intensity measurements for aerosol correction,
605 *Atmospheric Measurement Techniques*, 3, 1287-1305, 2010.
- Wagner, T., Dix, B., Friedeburg, C. v., Frieß, U., Sanghavi, S., Sinreich, R., and Platt, U.: MAX-DOAS
O₄ measurements: A new technique to derive information on atmospheric aerosols -- Principles and
information content, *J. Geophys. Res.*, 109, D22205, 10.1029/2004jd004904, 2004.
- Wagner, T., Ibrahim, O., Shaiganfar, R., and Platt, U.: Mobile MAX-DOAS observations of tropospheric
610 trace gases, *Atmos. Meas. Tech.*, 3, 129-140, 2010a.
- Wagner, T., Ibrahim, O., Shaiganfar, R., and Platt, U.: Mobile MAX-DOAS observations of tropospheric
trace gases, *Atmos. Meas. Tech.*, 3, 129-140, 10.5194/amt-3-129-2010, 2010b.
- Wang, S., Zhou, B., Wang, Z., Yang, S., Hao, N., Valks, P., Trautmann, T., and Chen, L.: Remote sensing
of NO₂ emission from the central urban area of Shanghai (China) using the mobile DOAS technique,
615 *Journal of Geophysical Research: Atmospheres*, 117, D13305, 10.1029/2011jd016983, 2012.
- Wang, Y., McElroy, M. B., Martin, R. V., Streets, D. G., Zhang, Q., and Fu, T.-M.: Seasonal variability
of NO_x emissions over east China constrained by satellite observations: Implications for combustion
and microbial sources, *Journal of Geophysical Research*, 112, 10.1029/2006jd007538, 2007.



- Wittrock, F., Oetjen, H., Richter, A., Fietkau, S., Medeke, T., Rozanov, A., and Burrows, J.: MAX-DOAS
620 measurements of atmospheric trace gases in Ny-Ålesund-Radiative transfer studies and their
application, *Atmos. Chem. Phys.*, 4, 955-966, 2004.
- Wu, F., Xie, P., Li, A., Mou, F., Chen, H., Zhu, Y., Zhu, T., Liu, J., and Liu, W.: Investigations of temporal
and spatial distribution of precursors SO₂ and NO₂
vertical columns in the North China Plain using mobile DOAS, *Atmospheric Chemistry and Physics*,
625 18, 1535-1554, 10.5194/acp-18-1535-2018, 2018.
- Zhang, Q., Streets, D. G., He, K., Wang, Y., Richter, A., Burrows, J. P., Uno, I., Jang, C. J., Chen, D., Yao,
Z., and Lei, Y.: NO_x emission trends for China, 1995–2004: The view from the ground and the view
from space, *Journal of Geophysical Research*, 112, 10.1029/2007jd008684, 2007.
- Zhang, Q., Streets, D. G., Carmichael, G. R., He, K. B., Huo, H., Kannari, A., Klimont, Z., Park, I. S.,
630 Reddy, S., Fu, J. S., Chen, D., Duan, L., Lei, Y., Wang, L. T., and Yao, Z. L.: Asian emissions in 2006
for the NASA INTEX-B mission, *Atmos. Chem. Phys.*, 9, 5131-5153, 2009.
- Zhang, Q., Geng, G., Wang, S., Richter, A., and He, K.: Satellite remote sensing of changes in NO_x
emissions over China during 1996–2010, *Chinese Science Bulletin*, 57, 2857-2864, 10.1007/s11434-
012-5015-4, 2012.
- 635 Zhang, X. Y., Sun, J. Y., Wang, Y. Q., Li, W. J., Zhang, Q., Wang, W. G., Quan, J. N., Cao, G. L., Wang,
J. Z., Yang, Y. Q., and Zhang, Y. M.: Factors contributing to haze and fog in China, *Chin. Sci. Bull.*
(Chin. Ver.), 58, 1178-1187, 2013.
- Zhao, B., Wang, P., Ma, J. Z., Zhu, S., Pozzer, A., and Li, W.: A high-resolution emission inventory of
primary pollutants for the Huabei region, China, *Atmospheric Chemistry and Physics*, 12, 481-501,
640 10.5194/acp-12-481-2012, 2012.
- Zyrichidou, I., Koukouli, M. E., Balis, D., Markakis, K., Poupkou, A., Katragkou, E., Kioussioukis, I.,
Melas, D., Boersma, K. F., and van Roozendaal, M.: Identification of surface NO_x emission sources
on a regional scale using OMI NO₂, *Atmospheric Environment*, 101, 82-93,
10.1016/j.atmosenv.2014.11.023, 2015.
- 645



650 Table 1. Sampling periods of the car MAX-DOAS experiment and corresponding meteorological conditions over Beijing in January, September, and October, 2014.

Journey	Date	Time (BJT)	Wind speed (m/s)	Type of wind field*	Total cloud fraction	PBL Height (m)
1**	2014/1/18	10:48-13:09	2	O	0	564
2	2014/1/19	13:31-15:40	1	O	7	167
3	2014/1/21	13:15-15:32	3	S	0	163
4	2014/1/23	10:39-12:25	3	O	7	187
5	2014/1/23	13:07-15:12	2	O	7	163
6	2014/1/24	10:42-12:03	2	N	8	39
7	2014/1/24	13:03-15:09	3	N	8	39
8**	2014/1/26	10:21-12:13	5	S	5	341
9**	2014/1/27	09:11-11:38	2	O	7	75
10**	2014/1/27	13:30-15:28	2	O	0	178
11**	2014/9/14	09:40-12:52	4	N	10	173
12**	2014/9/14	15:02-17:17	2	N	10	226
13**	2014/9/17	09:07-11:42	2	O	7	173
14	2014/9/19	09:09-11:50	2	S	3	178
15	2014/10/9	13:04-14:44	1	S	7	43
16	2014/10/10	09:52-12:28	2	S	7	663
17**	2014/10/12	14:02-16:42	3	N	7	167
18**	2014/10/13	09:12-11:59	3	O	0	186
19**	2014/10/13	13:11-16:27	3	O	0	130

*Three types of wind filed are South (S), North (N) and Other (O).

**The data from ten circling journeys are used to estimate the NO_x emission.

655

660

665

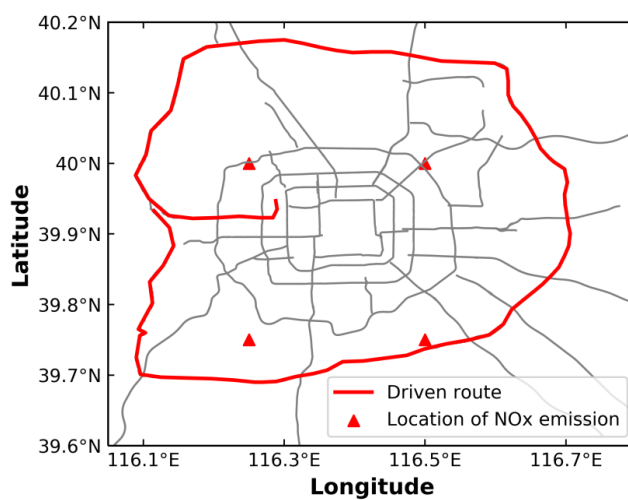


Fig. 1 Driving routes (red line) of the car MAX-DOAS experiment on the 6th Ring Rd of Beijing.

670

675

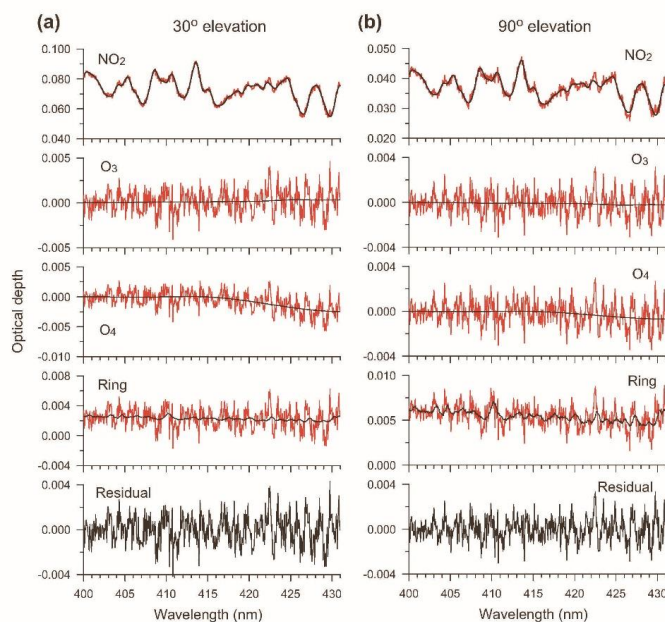


Fig. 2 Examples of the NO_2 retrieval from two successive spectra measured **(a)** at a 30° elevation angle (with NO_2 differential slant column density (DSCD) of 1.23×10^{17} molecules cm^{-2}) and **(b)** at a 90° elevation angle (with NO_2 DSCD of 6.22×10^{16} molecules cm^{-2}) on January 18, 2014, at around 11:40 BJT.

685

690

695

700



705

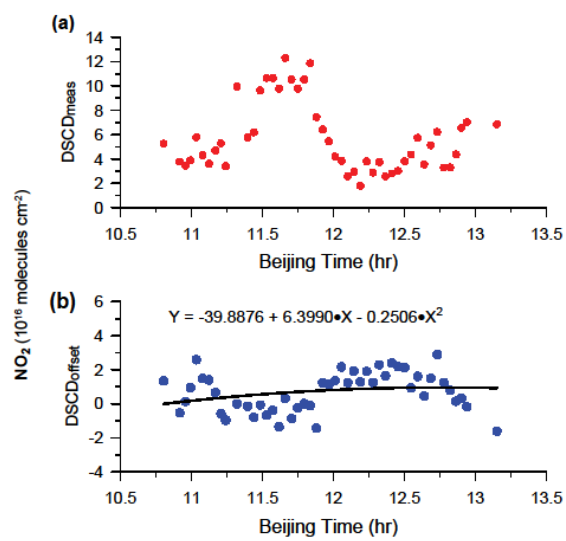


Fig. 3 Time series of the NO₂ (a) DSCD_{means} (red dots) and (b) DSCD_{offset} (black dots) (units of 10¹⁶ molecules cm⁻²) for the 30° elevation angle of each sequence on January 18, 2014. The black curve represents a second-order polynomial fit from individual DSCD_{offset} data points.

710

715

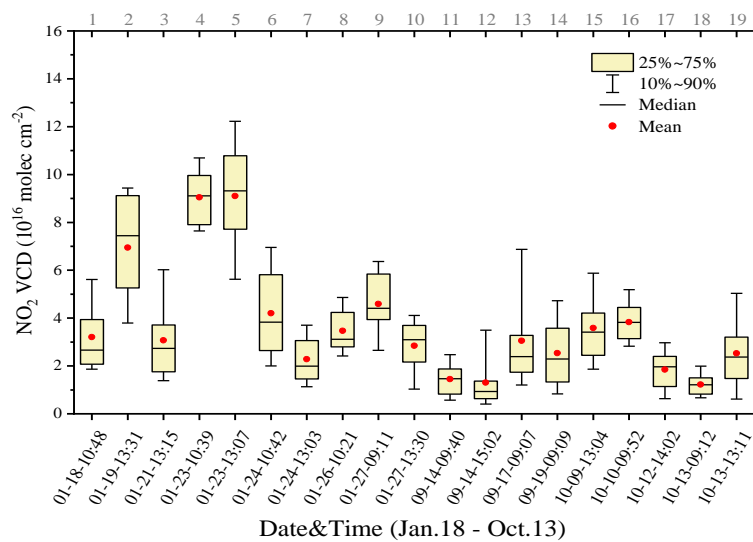


Fig. 4 Time series of the tropospheric NO₂ vertical column density (VCD) for 19 circling journeys on the Sixth Ring Road of Beijing in January, September, and October, 2014. Lower (upper) error bars and yellow boxes are the 10th (90th) and 25th (75th) percentiles of the data of each journey, respectively. Hyphens inside the boxes are the medians, and red circles are the mean values. The numbers of each journey are labeled at the top axis. See Table 1 for detailed information about each journey.

725

730

735

740



745

750

755

760

765

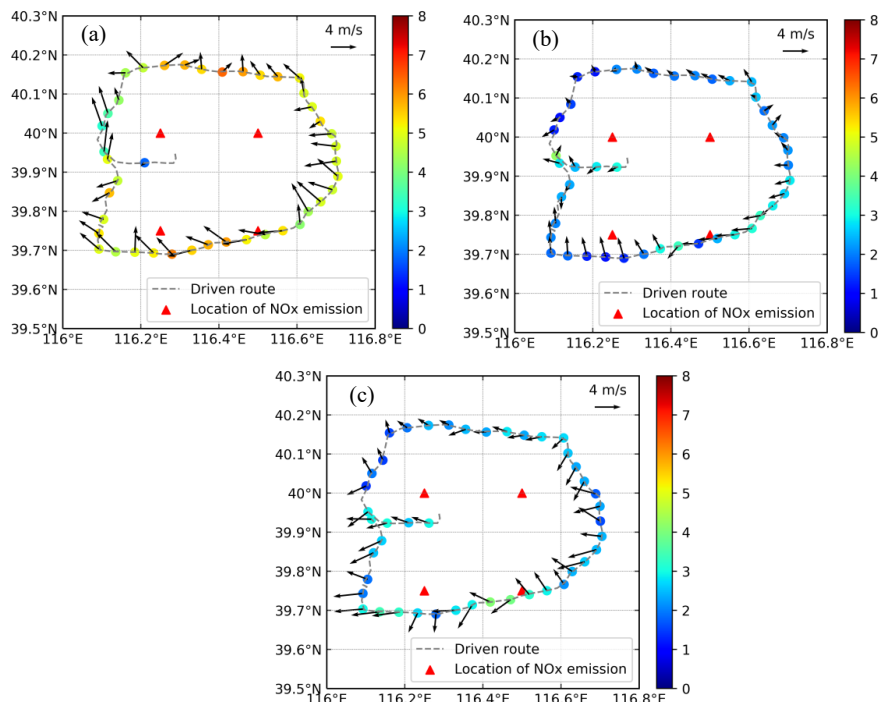


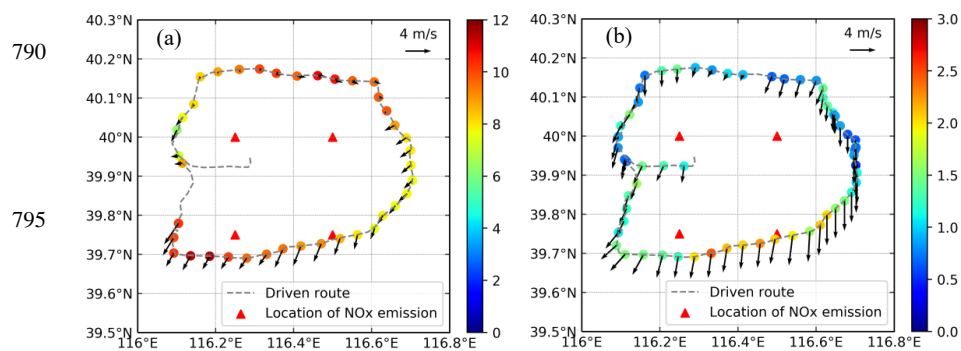
Fig. 5 Distributions of the monthly average NO₂ VCD (E16 molecules cm⁻²) on the 6th Ring Rd of Beijing in (a) January, (b) September, and (c) October, 2014.

770

775

780

785



800 **Fig. 6** Distributions of the maximum and minimum NO_2 VCD ($\text{E16 molecules cm}^{-2}$) on the 6th Ring
805 Rd of Beijing on the morning of (a) January 23 and (b) October 13, 2014.

810

815

820

825



830

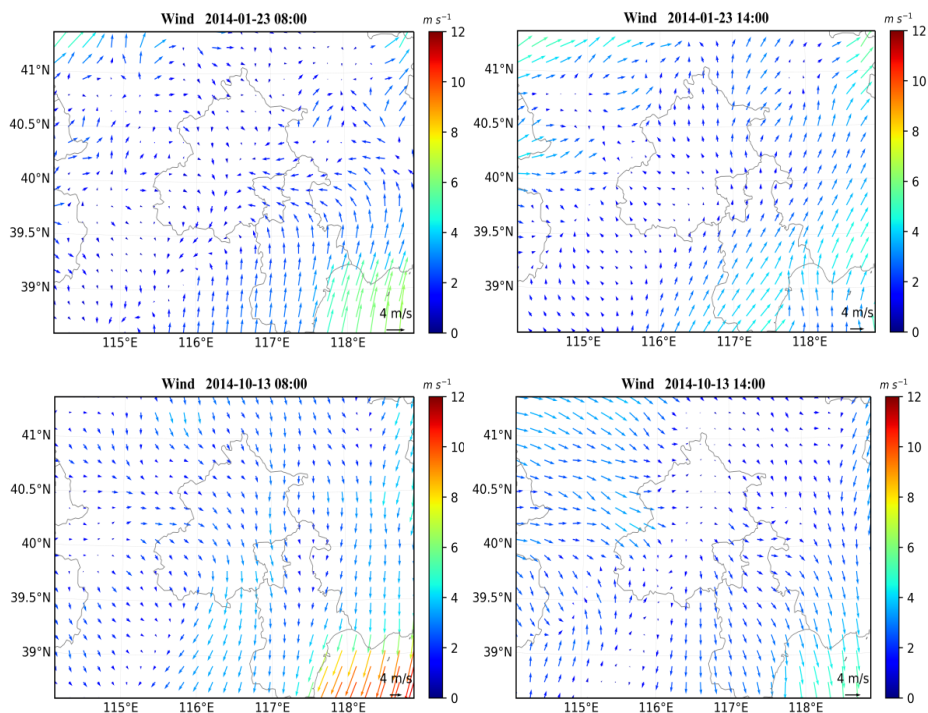


Fig. 7 Wind fields in Beijing and the surrounding area from ECWRF at 08:00 (left column) and 14:00 (right column) BJT on January 23 and October 13, 2014.

835

840

845

850

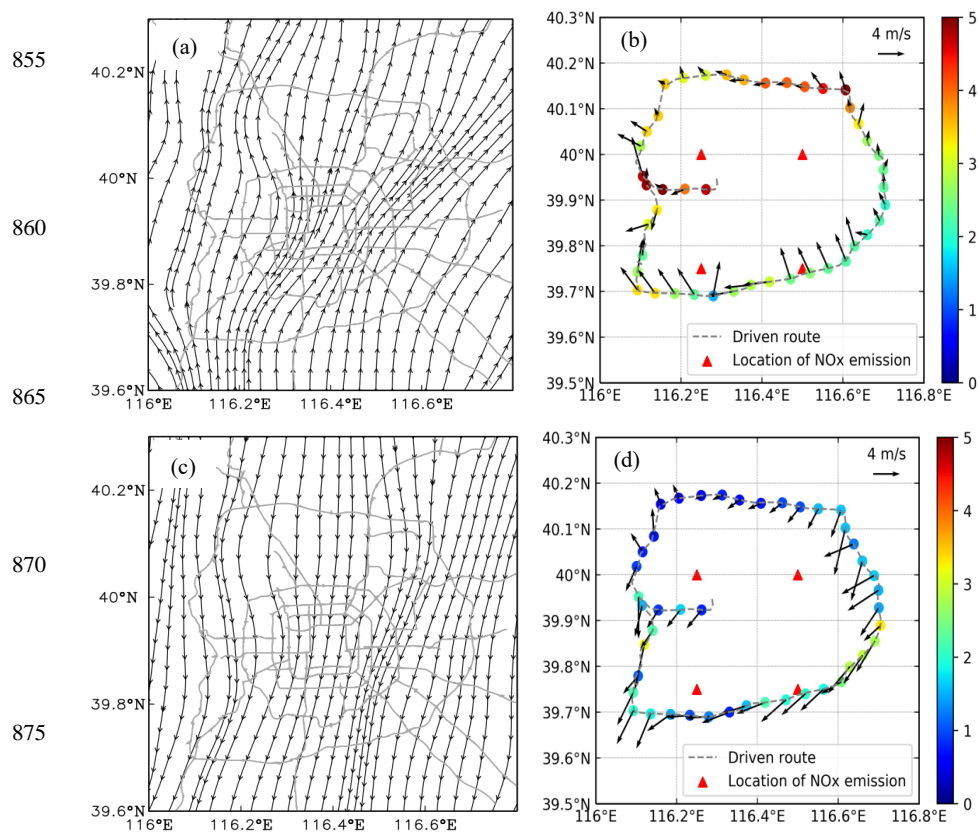


Fig. 8 Average wind stream and NO₂ VCD (E16 molecules cm⁻²) distributions under the three different types of wind field over Beijing: (a) south wind, (b) NO₂ VCD under south wind, (c) north wind, and (d) NO₂ VCD under north wind.

885

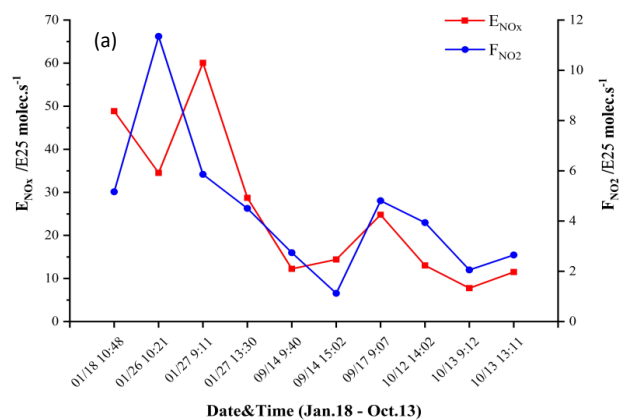
890



895

900

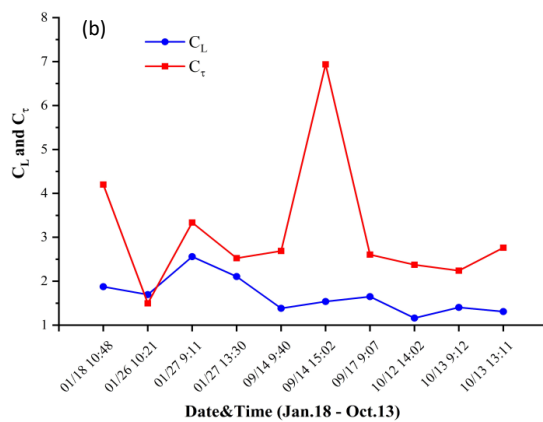
905



910

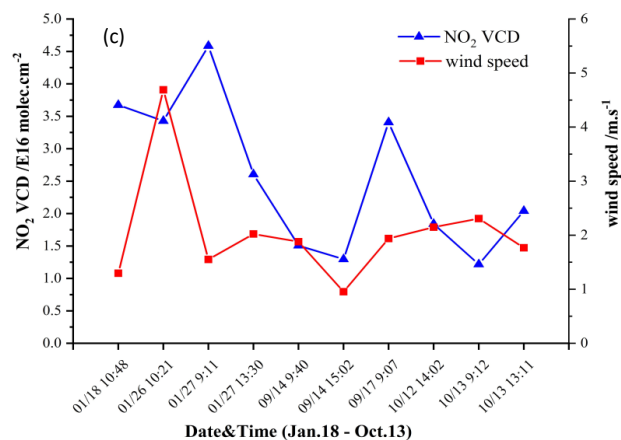
915

920



925

930



935

Fig. 9 Journey-to-journey variation in (a) F_{NO_2} and E_{NO_x} , (b) c_τ and c_L , (c) NO_2 VCD and mean wind speed for 10 circling journeys on the 6th Ring Rd of Beijing in January, September, and October, 2014.

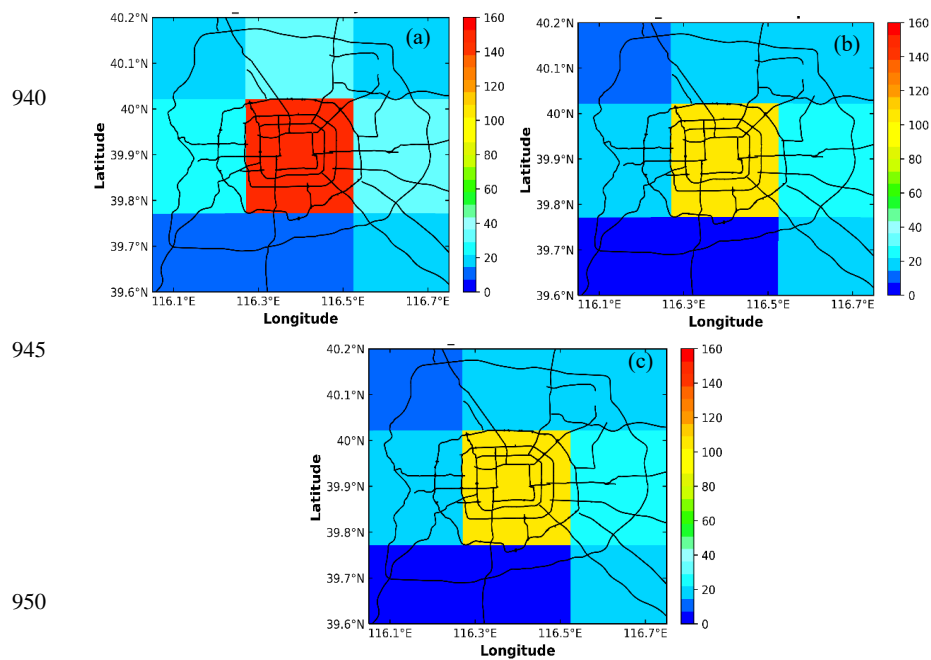


Fig. 10 Spatial distributions of NO_x emissions ($\text{mole km}^{-2} \text{h}^{-1}$) over Beijing based on the MEIC inventory in (a) January, (b) September, and (c) October 2012.

955

960

965

970



975

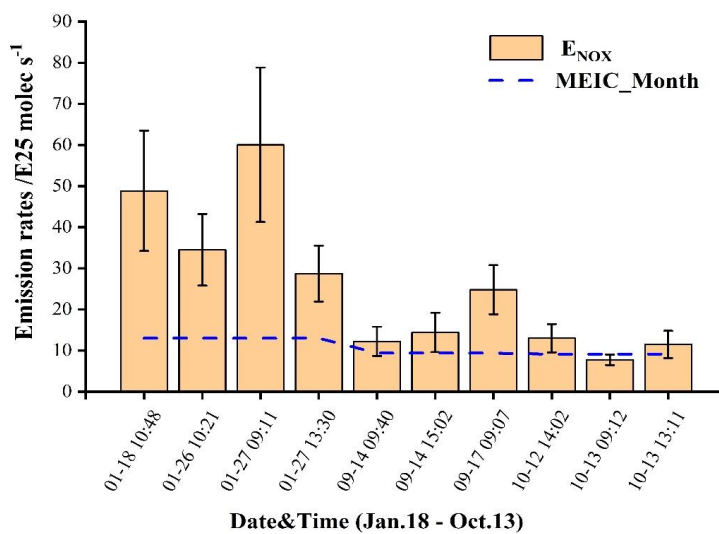


Fig. 11 Journey-to-journey variation in estimated E_{NO_x} and corresponding monthly emissions rates from the MEIC inventory (MEIC_Month) within the 6th Ring Rd of Beijing in January, September, and October 2014. Error bars represent the uncertainties in estimated E_{NO_x}

980

985

990

995

1000